International Journal of Engineering

Journal Homepage: www.ije.ir

Cogging Torque Minimization in Transverse Flux Permanent Magnet Generators using Two-step Axial Permanent Magnet Segmentation for Direct Drive Wind Turbine Application

R. Nasiri-Zarandi*[a], A. Mohammadi Ajamloo[b], K. Abbaszadeh[b]

[a] *Electrical Machine Group, Niroo Research Institute (NRI), Tehran, Iran*
[b] *Department of Electrical Engineering, K.N. Toosi University of Technology, Tehran, Iran*

PAPER INFO

Paper history:
Received 19 June 2019
Received in revised form 18 October 2020
Accepted 04 November 2020

Keywords:
Cogging Torque
Design of Experiment
Magnetic Equivalent Circuit
Permanent Magnet
Permanent Magnet Segmentation
Taguchi Method
Transverse Flux Machine
Wind Turbine

ABSTRACT

Transverse flux permanent magnet machines (TFPMs) are categorized as synchronous machines that benefit from having high value of torque density and capablity of accommodating high pole numbers. These characteristics make TFPMs suitable candidates for low-speed applications where high torque density value is requred such as direct drive wind turbine application. Despite the aforementioned advantages, TFPMs suffer from intrinsically high cogging torque value which is an important concern for wind turbine application. This paper focuses on axial PM segmentation technique to minimized cogging torque of TFPM topologies. Concept of the proposed method is discussed using analytical equations and optimum segmentaion angle is formulized. Non-linear magnetic equivalent circuit (MEC) is adopted where the PM segmentation, armature reaction, rotor transition and iron saturation effect are carefully modeled. The results of the MEC simulation are compared with the finite element method (FEM) results in terms of accuracy and computational time. The results from the analysis indicate that the proposed MEC method is almost ten times faster than FEM with reasonable level of precision. Taguchi method is adopted as a fast-response optimization method to improve the generator torque characteristics. The results show that the cogging torque has reduced by 97% with respect to the initial design while the average torque has only dropped by 8% which is an acceptable side effect due to the significant improvement in machine cogging torque.

doi: *10.5829/ije.2021.34.04a.17*

1. INTRODUCTION

The gearbox and transmission equipment in wind turbine systems reduce the efficiency of the wind generation system [1]. Furthermore, the gearing system reduces the reliability of the wind turbine and requires periodic maintenance [2, 3]. The absence of transmission equipment is considered an advantage for the direct-drive wind turbines (DDWTs), however, some considerations need to be taken into account. Owing to the elimination of the gearing system in DDTWs, the generator rotational speed is reduced with respect to the geared systems. Generally, in rotating electrical machines, the speed and volume are inversely proportional (at constant electrical and magnetic loadings). Consequently, in DDWT systems, the volume and weight of the generator increase, significantly. These problems result in increased generator manufacturing cost and stronger and expensive tower structure. Therefore, a generator with a high value of torque density is needed in DDWT systems [4]. In wind turbine systems, especially in DDWTs, generator cogging torque is an important criterion that must be taken into consideration. This is due to the fact that high values of the cogging torque prevent the turbine from starting up in low-speed wind [5]. Additionally, cogging torque and torque ripple induce noticeable noise and vibration to the structure [6–8]. So, based on the aforementioned discussion, two crucial characteristics of DDWT generators are: having high-value torque density and low value of cogging torque.

*Corresponding Author Institutional Email: *RNasiriZarandi@nri.ac.ir* (R. Nasiri-Zarandi)

Please cite this article as: R. Nasiri-Zarandi, A. Mohammadi Ajamloo, K. Abbaszadeh, Cogging Torque Minimization in Transverse Flux Permanent Magnet Generators using Two-step Axial Permanent Magnet Segmentation for Direct Drive Wind Turbine Application, International Journal of Engineering, Transactions A: Basics Vol. 34, No. 04, (2021) 908-918

Transverse flux permanent magnet machines (TFPMs) are categorized as synchronous machines which benefit from having a high value of torque density and capability of accommodating a high number of poles. These characteristics make TFPMs potential candidates for DDWT systems [9]. Generally, in TFPMs, the number of rotor poles are integer multiples of stator teeth which results in a considerably high value of cogging torque [10]. To this end, cogging torque minimization of TFPMs is discussed in many kinds of researches. Skewing stator U-I cores are investigated in [11] and effective results are presented. However, considering the laminated structure of U-I cores, shaping the proposed skewed parts is a very difficult procedure in practice. Optimizing the PM dimension is carried out in [12] to reduce the cogging torque of the tubular TFPM. However, the cogging torque reduction resulted from this technique is very weak. Unequal pole pitch of the rotor poles is studied in [13] and a noticeable reduction in cogging torque along with improvement in voltage harmonic components is achieved. However, the average electromagnetic torque has been reduced in this technique. Using different Halbach–Array structures to minimize the cogging torque is studied in [14, 15] and promising results are presented. However, the manufacturing process of Halbach-Array TFPM is relatively complicated. Shifting and unequal width of stator teeth is discussed in [16] which effective results along with experimental validations are presented. However, the proposed technique is not applicable to all TFPM topologies and is mainly applicable to certain topologies which use expensive SMC cores.

Generally, three phases TFPMs are built in three separate modules where each module belongs to a certain phase. In this case, three separate phases with almost zero magnetic couplings among them are developed. The stator of the TFPM topology is mainly developed based on using U and I-shaped laminated cores. The rotor of the earliest generation of the TFPMs contained two rows of PMs in each phase placed on an iron yoke. The stator was composed of only U-shaped laminated cores surrounding a circumferential winding [17]. The problem was that only half of the PMs contributed to useful power production while the other half created leakage flux and even reduced the useful power [17]. The above-mentioned deficiency was partially overcome by adding I-shaped laminated cores beside U-cores. By adding the I-shaped cores, the other half of PMs were shunted and didn't create the leakage flux, but still, these PMs couldn't produce useful power. To bring all the PMs into process of useful power production, the rotor yoke was separated into upper and lower rows [18]. By applying this modification, full utilization of PMs was achieved since all PMs were brought into the main flux path as shown in Figure 1. Regarding this figure which presents one pole pair flux path of the TFPM, it is seen that the flux path has three dimensional (3D) nature. Therefore, analysis of TFPM topologies requires the 3D finite element method (FEM). FEM is a popular solution with a high level of accuracy and is extensively used in 2D and 3D analysis [19, 20]. However, applying 3D FEM is a time taking process especially for optimization purposes. Thus, many papers investigated using alternative analysis tools to substitute for the time-consuming FEM. The magnetic equivalent circuit (MEC) method has been considered as a potential substitute for the FEM due to its fast computational process and acceptable level of accuracy [21, 22]. It needs to be stated that getting an acceptable level of accuracy from the MEC method requires precise modeling of iron non-linearity, fringing flux, air gap permeances, and rotor transition which are taken into account in this study.

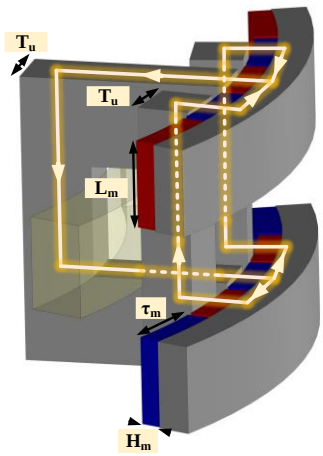

Figure 1. Main flux path of a single-phase TFPM in one pole pair

In this paper, aiming to minimize the cogging torque of a 2 kW TFPM, a two-step PM segmentation technique is proposed. Axial PM segmentation concept is explained and the related formulation is extracted to achieve a global formula for finding the optimum segmentation angle. To reduce the processing time of the analysis, a non-linear dynamic MEC model is developed and its results are validated by FEM. To improve the torque characteristics (electromagnetic and cogging torques) of the TFPM, fast-computing design of experiments (DOE) optimization is used based on the Taguchi method.

2. PM SEGMENTATION CONCEPT IN TFPMS

Ideally, three phase TFPMs are considered as three separate modules with no magnetic coupling among the phases (modules). However, small magnetic leakage flux between modules may exist resulting a magnetic coupling between the adjacent modules. However, this leakage flux is very weak which can be neglected in the

analysis. So, by assuming three magnetically decoupled modules, cogging torque of Three-phase TFPMs is calculated for each module (i.e. phase A), independently. Then, cogging torque waveforms of phase B and C are obtained by shifting the cogging torque waveform of phase A by ±120° electrical degree. Consequently, the cogging torque of a three-phase TFPM is developed as in Equation (1);

$$T_{cog} = \sum_{n=1}^{\infty} a_n[\sin(n\theta_e) + \sin(n(\theta_e + \frac{2\pi}{3})) + \sin(n(\theta_e - \frac{2\pi}{3}))] \quad (1)$$

Here, the cogging torque of each phase is written in the form of the Fourier series where the first, second, and third terms belong to phase A, B, and C respectively.

So, it can be understood from Equation (1) that in a TFPM with three separate phases, all the cogging torque harmonic components are canceled in a three-phase cogging torque waveform except multiples of the third component. Actually, multiples of the third components due to obtaining the same phase are tripled in the three-phase waveform. Evidently, in a three-phase cogging torque waveform, the major harmonic component is one of the multiples of the third harmonic component. So, identifying the major harmonic component and minimizing it is pursued. To achieve such a goal, the technique of axial PM segmentation is proposed.

In this regard, Figure 2 represents the PM arrangement of TFPM before and after PM segmentation. According to Figure 2(b), two-step PM Segmentation is adopted where each PM is split into two upper and lower PMs which are shifted by a specific angle (φ_m) with respect to upper PM. Consequently, a single-phase cogging torque waveform could be written in a Fourier series of Equation (2).

$$T_A = \sum_{n=1}^{\infty}[a_n \sin(n\theta_e) + a_n' \sin(n(\theta_e + \frac{p}{2}\varphi_m))] \quad (2)$$

Here, the first term represents the effect of the upper PMs and the second term represents the lower PMs which are shifted by an angle of φ_m with respect to upper PMs. Here, p is the number of poles.

Regarding Equation (2), if the effects of fringing and leakage fluxes are neglected, an and a_n' can be assumed equal. So, it is possible to select a desired harmonic component from the single-phase cogging torque waveform and eliminate it by adjusting the shifting angle (φ_m). It means that the dominant component of the three-phase cogging torque waveform (i.e. i^{th} component) could be theoretically suppressed by choosing a specific shift angle as in Equation (3);

$$T_i = a_i \sin(i\theta_e) + a_i \sin(i(\theta_e + \frac{p}{2}\varphi_m)) = 0 \quad \Rightarrow \varphi_m = \frac{360^0}{ip} \quad (3)$$

To analyze the proposed solution, a 2 kW TFPM generator with a rated speed of 350 rpm is designed for the DDWT application where its specifications are listed in Table 1. The detailed design procedure is presented in the next section. In Figure 3, cogging torque waveforms of single-phase and three-phase TFPM are depicted. As stated earlier, the three-phase cogging torque is developed by adding three single-phase waveforms that have 120° electrical degree shift angles.

Harmonic components of the single-phase and three-phase cogging torque waveforms are extracted and shown in Figure 4. Accordingly, the 2nd, 4th, and 6th components are the dominant components in single-phase cogging torque waveform. The 8th, 10th, and 12th components are minor harmonic components while the other harmonics components are negligible.

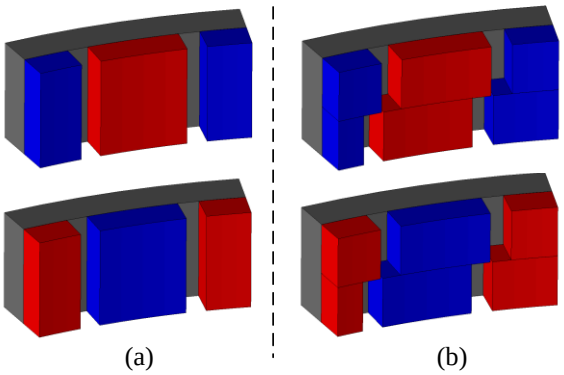

Figure 2. One pole pair view of PM configurations in (a) conventional TFPM topology, and (b) the proposed two-step axially segmented TFPM topology

TABLE 1. Design specifications of proposed TFPM

Parameter	Symbol	Value	Unit
Output power	P	2000	W
Nominal speed	n	350	rpm
No. of phases	m	3	---
No. of poles	p	40	---
Air gap diameter	D_g	203	mm
Rotor outer diameter	D_o	225	mm
Machine length	L	180	mm
Air gap length	g	1	mm
Stator shoe width	T_u	10.5	mm
PM length	L_m	15	mm
PM thickness	d_m	4	mm
Number of armature turns per phase	N	158	---
PM coercive force	H_c	-880	kA/m
PM residual flux density	B_r	1.25	T

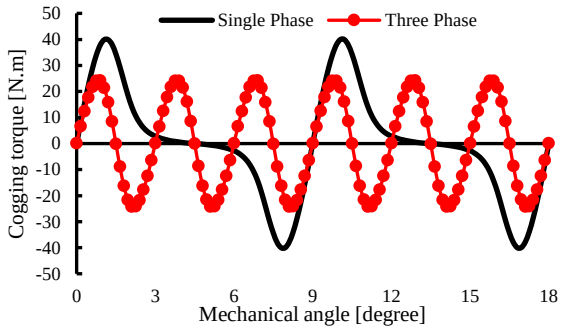

Figure 3. Single-phase and three-phase cogging torque waveforms of the TFPM generator

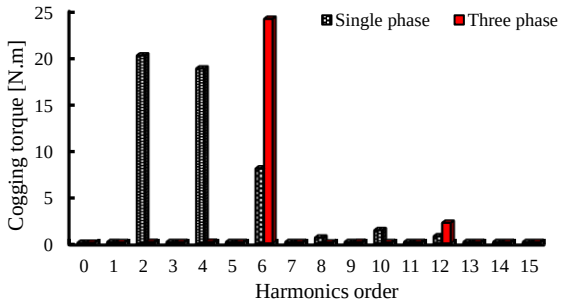

Figure 4. Cogging torque harmonics components of single-phase and three-phase TFPM generator

Since all the harmonic components except multiples of 3 are eliminated in the three-phase waveform, the 6th harmonics component is the dominant component in three-phase TFPM. In fact, its amplitude is three times of the 6th component of the single-phase machine. The other noticeable component is the 12th component which is not comparable to the 6th component. Consequently, the cogging torque of the three-phase TFPM is mainly determined by the 6th harmonics component. So, the cogging torque of the three-phase TFPM can be minimized by minimizing the 6th harmonic component. To do so, axial PM segmentation is adopted with a segmentation angle of φ_m. In this regard, Equation (4) should be solved. In this equation, the first term represents the torque component of the upper PMs and the second term represents it for the lower PMs.

$$T_{n=6} = a_6 \sin(6\theta_e) + a_6' \sin(6(\theta_e + \frac{40}{2}\varphi_m)) = 0 \quad (4)$$

By considering a_6 and a_6' as equal parameters and solving Equation (4), the possible values of shifting angles are determined as in Equation (5).

$$\varphi_m = 1.5 \times k \quad , \quad k = 1,3,5,... \quad (5)$$

It is revealed from Equation (5) that ideally the 6th harmonic component of the cogging torque waveform is canceled if by choosing the shift angle as one of the following values; 1.5, 4.5, 7.5, etc.

To evaluate the validity of the above-mentioned solution, peak to peak value of the three phase cogging torque waveform is calculated using FEA at different shift angles. The results of such analysis are extracted and presented in Figure 5. It is noticed that by increasing the shifting angle, the torque reduces and reaches the minimum value at the angle of 1.5 degrees. At this point, the 6th harmonic component has the minimum value leading to the minimum cogging torque. By further increasing the shift angle, the cogging torque increases and reaches the peak value at the angle of 3 degrees. According to Equation (4), at this angle, the 6th harmonic component of cogging torque for top and bottom PMs are in the same phase angle which results in peak cogging torque value. By increasing the segmentation angle until 4.5 degrees, the cogging torque reduces to its minimum value. The cogging torque waveform of the TFPM is presented in Figure 6 for 0 and a 1.5-degree segmentation angle. The comparison shows that the cogging torque decreases by more than 85%. Figure 7 indicates harmonic components of the single-phase TFPM at 0 and 1.5-degree segmentation angles. The 6th harmonic component which mostly determines the three-phase cogging torque has decreased to 13% after the adoption of a 1.5-degree segmentation angle. Moreover, the 12th harmonic component has decreased by 20%.

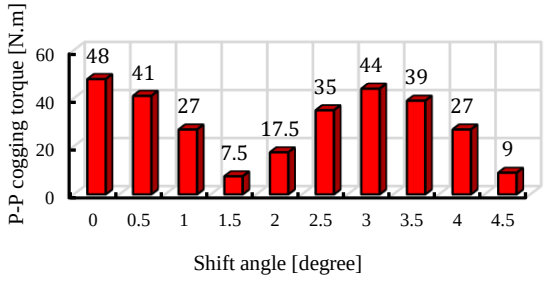

Figure 5. Peak to peak cogging torque values for three-phase TFPM versus axial segmentation angle

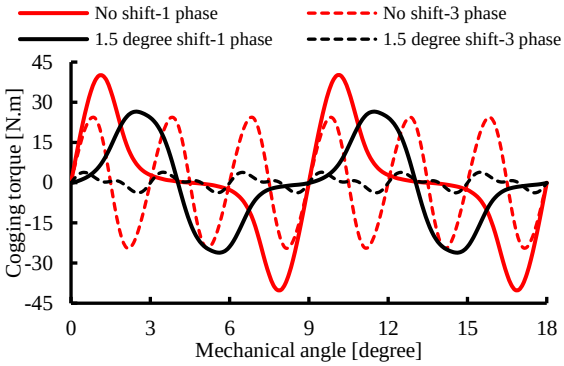

Figure 6. Single-phase and three-phase cogging torque waveforms of the TFPM generator at two segmentation angles

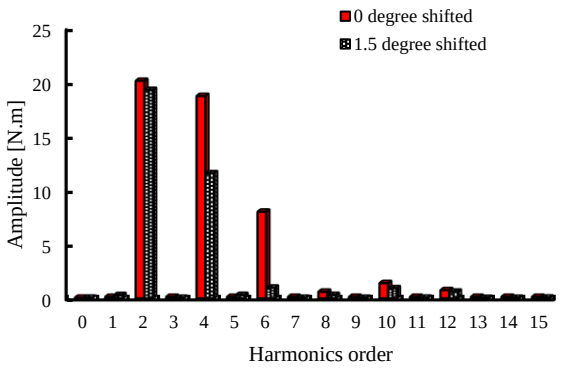

Figure 7. Harmonic components of single-phase TFPM at two segmentation angles

In this section, the PM segmentation concept was explained in TFPM topologies. Related formulations were extracted and optimum shift angles are formulized to achieve a minimum cogging torque value. By selecting a 1.5-degree segmentation angle 6th component of the cogging torque which is the dominant component of the cogging torque waveform reduces dramatically. So, it was revealed that after the adoption of this method the peak to peak value of three-phase cogging torque dropped from 48 N.m to 7.5 N.m. In the next section, the design and modeling algorithm of the TFPM generator is presented.

3. PROPOSING THE DESIGN ALGORITHM AND NON-LINEAR 3-D MEC

3. 1. Design Algorithm In Figure 8, the proposed design and modeling algorithm is presented. At the first step, machine rated parameters such as nominal power and terminal voltage are inserted. Next, machine design parameters such as electrical and magnetic loadings, air gap clearance, PM characteristics are set. Then, the initial assumptions for power factor, efficiency, and iron part potential drops are inserted. Afterward, the rotor pole arc length and coil turn number per phase are determined. Electrical loading of the TFPM generator is calculated as in Equation (6);

$$A_m = \frac{\sqrt{2} \times N \times I_a}{2 \times \tau} \tag{6}$$

Here, I_a is rms value of the rated armature current, N is the number of coil turn per phase and τ is the rotor pole arc length which is driven from Equation (7). By defining the pole arc length to pole axial length ratio (τ/L_m) as machine aspect ratio (β):

$$\tau = \sqrt[3]{\frac{E_f \times \beta \times I_a}{2 \times f \times p \times k_f \times B_{mg} \times A_m}} \tag{7}$$

where B_{mg} is the maximum flux density in the middle of the air gap, E_f is rms value of phase Back-emf, k_f is the

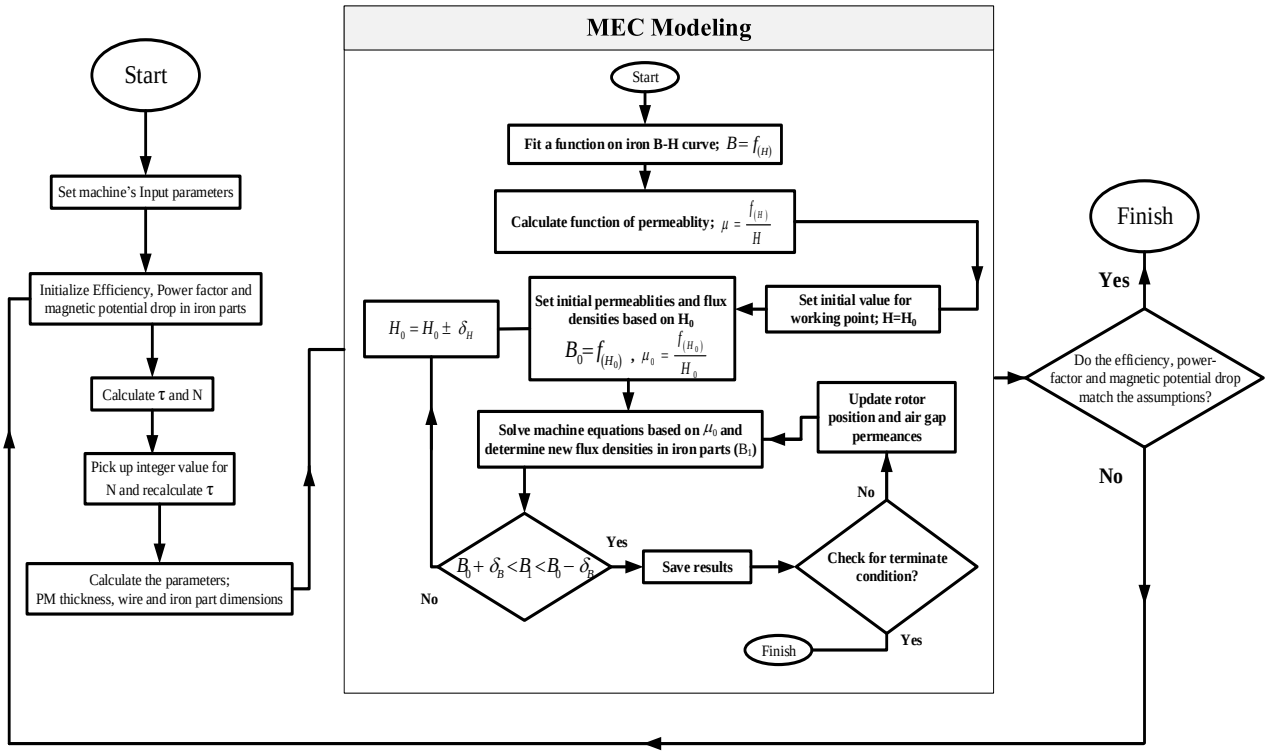

Figure 8. Proposed design algorithm of the TFPM coupled with non-linear MEC method

flux distribution factor, and f is the rated electrical frequency. After calculation of pole arc length, the number of coil turns is calculated using Equation (6). By rounding the value of N, the pole pitch is recalculated as in Equation (8).

$$\tau = \sqrt{\frac{E_f \times \beta}{\sqrt{2} \times f \times p \times k_f \times B_{mg} \times N}} \quad (8)$$

Based on Ampere's law in the main flux path of the magnetic circuit (Figure 1), the PM thickness is calculated as in Equation (9).

$$H_m = \frac{\mu_r B_{mg} \times g + 0.25\mu_0\mu_r \times V_{Fe}}{B_r - B_{mg}} \quad (9)$$

where, μ_r, B_r, g, and V_{Fe} are the PM relative permeability, PM residual flux density, air gap clearance, and the iron parts magnetic potential drop in one pole pair, respectively. Next, wire size, iron part dimensions such as the U-I thickness, rotor yoke thickness and window dimensions are calculated based on the initial inputs. At this step, an initial design for a TFPM is obtained. Now, the designed TFPM is analyzed using non-linear dynamic magnetic equivalent circuit method (MEC) which will be elaborated in the next subsection. After analyzing the TFPM using the MEC method, the algorithm checks if the assumed values of the efficiency, the power factor, and iron part potential drops are converged with the MEC results. If the assumed parameters converge with the MEC results, the output design is valid and the design procedure ends, otherwise, the assumed parameters are updated and the procedure goes on until the convergence results.

3. 2. Three Dimensional MEC Modeling In subsection 3.1, a detailed design algorithm of the TFPM generator was discussed. The proposed algorithm uses the non-linear MEC method to check the convergence of the design initial assumptions and the analysis results. So, accurate MEC modeling results in a more accurate design. Since, this study discusses the axial segmentation effect of the PMs on the cogging torque, the effect of two-step PM segmentation is included in the MEC method. In the proposed MEC method, effects of iron saturation, rotor movement, and fringing flux are also considered. The proposed MEC model will be used in the optimization procedure in the next section.

Two cross-sectional views of the TFPM reluctance network is presented in Figures 9(a) and 9(b). The front view of the proposed TFPM reluctance network is depicted in Figure 9(a) where the variable air gap reluctances are excluded. In this view, two-step PM segmentation is not visible while it is noticeable in the side view of Figure 9 (b). In this view, the I-shaped core is positioned behind the U-shaped core, consequently, the reluctance of this part is sketched using dotted lines (Figure 9 (b)).

3. 2. 1. General Equations Here, general equations of the MEC method are categorized as the followings:

PM Model: Each PM is modeled by a flux source shunted by a reluctance which represents the internal leakage of the PM. Corresponding values of the flux source and internal leakage reluctance are given in Equations (10) and (11), respectively.

$$F_1 = B_r \times L_m \times \tau_m \quad (10)$$

$$R_3 = \frac{d_m}{\mu_0\mu_r \times L_m \times \tau_m} \quad (11)$$

Armature MMF and Back-EMF: Armature reaction is modeled by MMF source. The flux linkage is the total

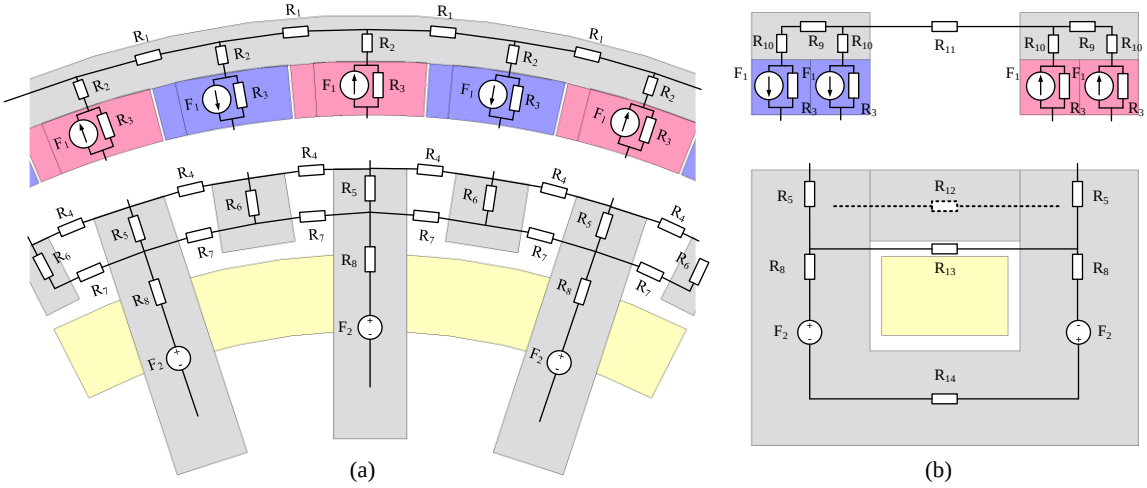

Figure 9. Reluctance network of the TFPM generator from two views, (a) front view, and (b) side view

flux which is in the same branch as the MMF source which determines the induced voltage in the coil as in Equation (12).

$$\begin{cases} F_2 = N \times I \\ \psi = N \times \phi \\ e = \dfrac{\partial \psi}{\partial t} \end{cases} \quad (12)$$

Torque Equation: According to literature [23, 24] the torque production is due to the change in the air gap permeance and the MMF drop on those permeances. So, for one phase of the TFPM the electromagnetic torque is calculated by Equation (13):

$$T = \sum_{i=1}^{n} U_i \times \frac{\partial G_i}{\partial \theta} \quad (13)$$

Here, G_i is the ith air gap permeance, U_i is MMF drop on it, θ is the rotor position, and n is the number of air gap permeances in each phase.

3. 2. 2. Variable Air Gap Permeance Model

The permeances between rotor poles and stator teeth are referred to as variable air gap permeances and are responsible for the energy conversion process. The air gap permeance modeling is based on the proposed model in literature [24]. The permeance model between one rotor pole (r_1) and one stator tooth (s_1) is presented in Figure 10. When the distance between the rotor pole and the stator tooth is as one pole pitch, the permeance is zero (Figure 10 (a)). By rotor movement and getting closer to stator teeth, the permeance increases until a complete overlap. This position is illustrated in Figure 10(b). By further movements of the rotor, the overlap is reduced and the permeance drops. It reaches zero when the position difference gets more than one pole pitch as presented in Figure 10(c). The transition of the permeance is assumed sinusoidal between G_{max} and zero. Consequently, the permeance between r_1 and s_1 is modeled as in Figure 10(d). The relevant parameters are defined as in Equation (14).

$$\begin{cases} a = \dfrac{2\pi}{p}, \ b = \dfrac{|\tau_m - T_u|}{D_g} \end{cases} \quad (14)$$

The value of variable air gap permeance is composed of two main components. The major component is caused by the overlapped area of the r_1 and s_1. Here, the flux path is straight and is illustrated in Figure 10 (e). The second component is due to the fringing flux and is presented in Figure 10(f), consequently, the maximum value of variable air gap permeance is calculated as in Equation (15) which the first term represents overlapping permeance and the second term represents the fringing permeance.

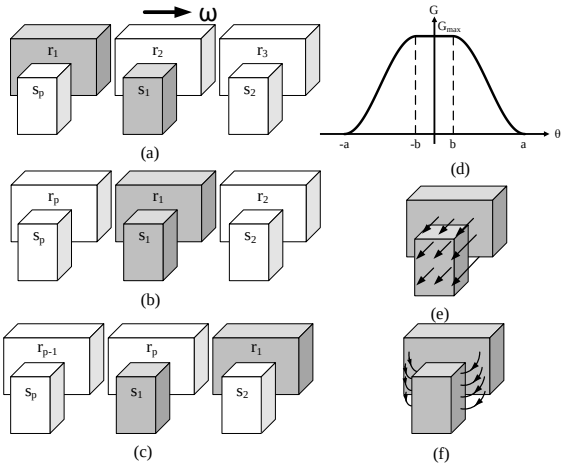

Figure 10. The variable air gap permeance between rotor pole (r_1) and stator tooth (s_1) at different angles, (a) angle of –a, (b) angle of zero, (c) angle of a, (d) Permeance model between r_1 and s_1, (e) Overlapping term of variable air gap permeance, and (f) Fringing term of variable air gap permeance

$$G_{max} = \left[\frac{\mu_0 L_m \times \min(\tau_m, T_u)}{g}\right] + \left[\frac{4\mu_0 L_m}{\pi} \times Ln(1 + \frac{\pi|\tau_m - T_u|}{4g})\right] \quad (15)$$

In the case of PM segmentation, each PM is axially divided into two PMs which the lower PM is shifted by the angle of θ_s. Consequently, if the permeance function between the top PM and the stator tooth (s_1) is $G_{(\theta)}$, then the permeance function between the bottom PM and the s1 is $G_{(\theta - \theta s)}$.

3. 2. 3. Iron Saturation Effect

To take the effect of iron saturation into account in the MEC model, the steel sheet B-H curve is split into four regions and a function is fitted per region. So, the steel B-H curve is estimated with a high level of precision using a piecewise function ($B=f_{(H)}$). Consequently, the permeability of the steel can be described by (16);

$$\mu = \frac{f(H)}{H} \quad (16)$$

At first, a random working point on the steel B-H curve is assumed for iron parts. Next, the corresponding reluctances are calculated for these parts based on the initial working point. Next, the reluctance network of the TFPM is solved and the magnetic flux densities of iron parts along with actual working point on steel B-H curve are obtained. The resulted working point is compared with the initial working point and if the difference is smaller than a specific value (δ_B), the results are saved and the next time step starts. Otherwise, the assumed working point is not valid, so the working point is changed till the difference between the initial and the resulted working points is smaller than the accepted error

(δ_B). Based on the aforementioned discussion, the algorithm of the non-linear dynamic MEC model is given in Figure 8.

3. 2. 4. MEC Results The torque and voltage waveforms of the 2kW TFPM are extracted using the proposed MEC method and compared with the FEM results in terms of precision and computational time. The no-load induced voltage waveform of the TFPM is calculated by both the MEC method and FEM and depicted in Figure 11. The result of the MEC method shows acceptable accuracy in calculating the Back-emf, since the point to point error is lower than 4%. Similarly, the cogging torque and the rated load torque are presented in Figure 12 and Figure 13, respectively. The comparison shows that the MEC method calculates the machine torque by less than 6% error in the worst case. The computational time of either method is also measured which reveals that the MEC method nearly 10 times faster than the FEM.

In this section, the design and modeling procedure of the TFPM generator was discussed. A comprehensive algorithm was proposed where the MEC method was adopted to increase the accuracy of the design procedure. The detail of the proposed MEC method was elaborated when modeling the effects of iron saturation, PM segmentation, and rotor movement were discussed. The results of the MEC were compared with the FEM results which both accuracy and computational speed of the proposed MEC method were proven. In the next section, the Taguchi optimization method is used to improve the torque characteristics of the designed TFPM generator.

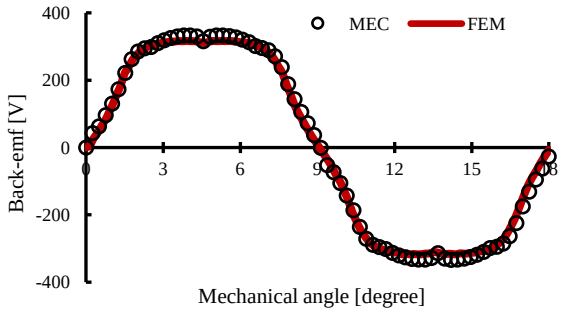

Figure 11. Back-emf waveforms of the TFPM generator at no-load condition resulted from the MEC method and FEM

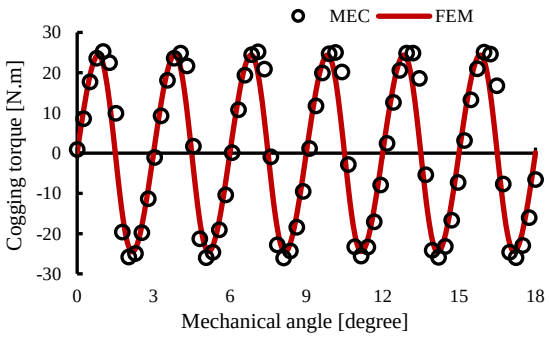

Figure 12. Cogging torque waveforms of the three-phase TFPM generator resulted by MEC method and FEM

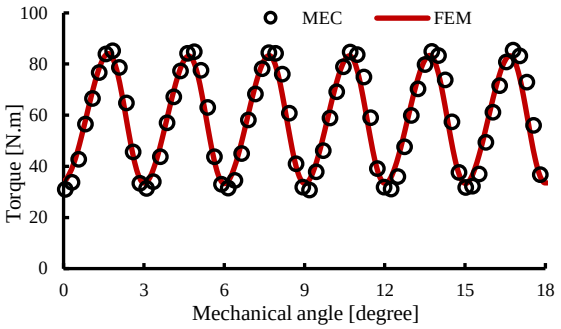

Figure 13. Electromagnetic torque waveform of the TFPM generator at rated load resulted by MEC and FEM

4. OPTIMIZATION OF TORQUE PROFILE

Until now, the PM segmentation procedure is discussed and the optimum shift angle between the upper and lower PM segments is formulated. Accordingly, the Optimum shift angle is fixed at 1.5 degrees (Equation (5)), and the sixth harmonic component which is the dominant component is minimized. Consequently, the peak cogging torque value of the TFPM has dropped from 24 N.m to 3.8 N.m after PM segmentation. To minimize the cogging torque as much as possible, the optimization method is used to optimize the machine parameters while the segmentation shift angle is fixed at its optimum value.

4. 1. Taguchi Optimization Method In this section, torque profiles of the 2 kW TFPM are optimized to improve its performance as a DDWT generator. Taguchi optimization method is selected as it is a popular and effective optimization method [25, 26]. Taguchi optimization method is one of the designs of experiments (DOE) methods which its accuracy, computational speed, and robustness have been proven. In an optimization problem, if there are 3 variables each at 5 levels, the full factorial design requires 5^3=125 experiments while the Taguchi method offers to perform only 25 experiments which leads to a considerable amount of computational effort.

4. 2. Optimization Procedure Aiming to minimize the cogging torque of the TFPM generator, 3 parameters each at 5 levels are chosen as optimization parameters. These variable parameters are as listed as following: stator pole shoe width (T_u), PM pole width to pole pitch ratio (α), and PM thickness (d_m).

Due to choosing 3 variables at 5 levels, the L_{25} orthogonal array is selected. At each experiment, cogging torque and the average torque are calculated and analyzed. In this study, achieving a minimum value for the ratio of cogging torque to average electromagnetic torque is the goal of the optimization.

4. 3. Optimization Results Figure 14 and Figure 15 represent the mean effect of variables on cogging torque and average torque, respectively. It is noticed that the first level of T_u, the third level of α, and the fifth level of d_m are the best combination which minimizes the cogging torque. From Figure 15, it is concluded that the average torque increases by increasing the variable levels. Hence, the combination of the fifth level of variables leads to the maximum value of average torque. Mean effect of the variables on cogging to average torque ratio which is the optimization goal is presented in Figure 16. As it can be noticed, the optimization function is minimized by choosing the 1st level of T_u, 3rd level of α, and 5th level of d_m. By selecting the aforementioned combination, and analyzing the final TFPM generator, the cogging torque waveforms are extracted and presented in Figure 17. The cogging torque of the final TFPM is reduced by 85% with respect to the non-optimized TFPM and 97% with respect to the initial design which is a dramatic reduction in generator cogging torque. The electromagnetic torque of the TFPM is also extracted at rated current compared with the non-optimized and initial designs (Figure 18). The comparison shows that the torque ripple of the TFPM after optimization has improved significantly. However, the average torque decreased by 8% with respect to the initial design and 5% with respect to the non-optimized TFPM. The mentioned decrease in the machine average torque is the most important side effect of the PM segmentation. The second side effect of the method is increased manufacturing complexity because of the two-step skew technique. In this way, instead of placing one PM per pole (conventional design), two PMs per pole are required where increases the manufacturing complexity of the machine. Nevertheless, losing 8% of the average torque and relatively higher complexity are tolerable considering a 97% decrease in the machine cogging torque which is a significant achievement compared to the existing methods in the literature. Finally, a cross-sectional view of the TFPM after 1.5 degrees PM segment shift and optimization procedure is presented in Figure 19. Contour and vector plots of magnetic flux density distribution in the TFPM along with the mesh plot of the TFPM are presented in Figure 19.

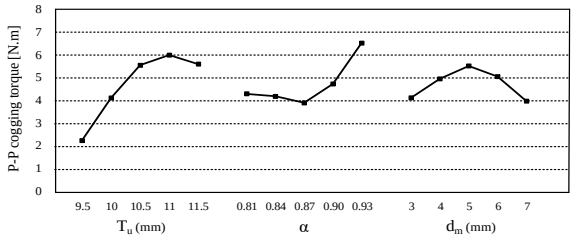

Figure 14. Mean effect of optimization variables on cogging torque of the three-phase TFPM generator

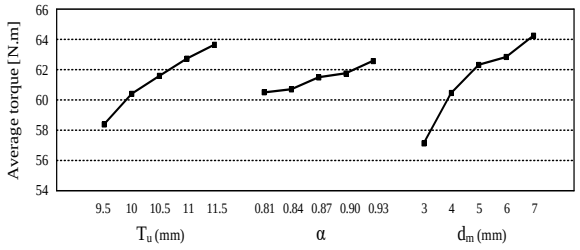

Figure 15. Mean effect of optimization variables on average torque of the three-phase TFPM generator

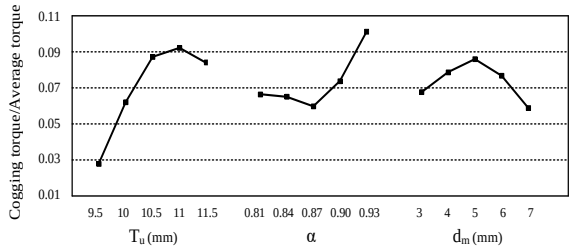

Figure 16. Mean effect of optimization variables on the ratio of TFPM cogging torque to average torque

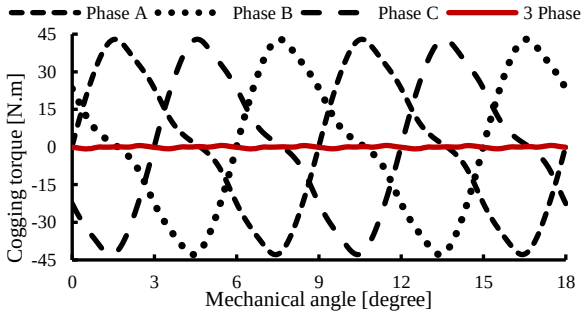

Figure 17. Single-phase and three-phase cogging torque waveforms of the optimized TFPM generator

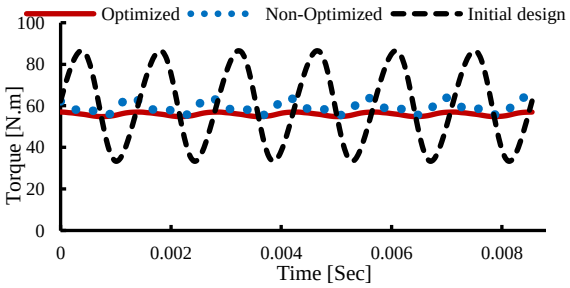

Figure 18. Electromagnetic torque of the three-phase TFPM generators at rated current

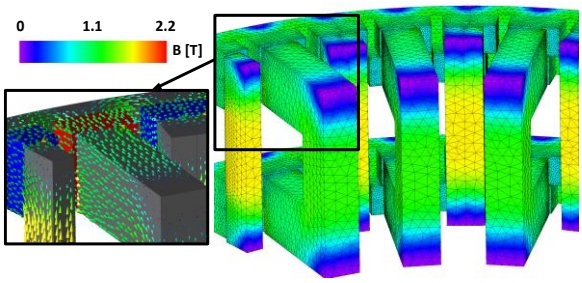

Figure 19. The cross-sectional view of the final TFPM generator along with vector and contour plots of magnetic flux density distribution

5. CONCLUSION

In this study, the optimum design of the TFPM generator for direct driven wind turbine application was addressed. Two steps axial PM segmentation concept in TFPMs was explained and the optimum shift angle was formulated. A non-linear dynamic MEC method was developed and a MEC based design algorithm for a two kW TFPM was presented. Results of the MEC were compared with the FEM results. The comparison showed that by replacing the MEC with the FEM, noticeable processing time was saved where acceptable level of accuracy was also resulted.

By adopting two step axial PM segmentation at the optimum segmentation angle, the cogging torque of the TFPM generator decreased by 85% with respect to the non-segmented generator. Taguchi optimization method was applied to minimize the ratio of cogging torque to average electromagnetic torque. The peak value of cogging torque was reduced from 24 N.m to 0.7 N.m after performing both the axial segmentation technique and Taguchi optimization method on the initial TFPM generator. Nevertheless, the generator torque rating was reduced by 8%. But, by considering the significant reduction in cogging torque (97%), losing 8% of generator rated torque can be easily tolerated.

6. REFERENCES

1. Sang-Yong Jung, Hochang Jung, Sung-Chin Hahn, Hyun-Kyo Jung, and Cheol-Gyun Lee, "Optimal Design of Direct-Driven PM Wind Generator for Maximum Annual Energy Production", ***IEEE Transactions on Magnetics***, Vol. 44, No. 6, (2008), 1062–1065. doi:10.1109/TMAG.2007.916250
2. McDonald, A., and Bhuiyan, N. A., "On the Optimization of Generators for Offshore Direct Drive Wind Turbines", ***IEEE Transactions on Energy Conversion***, Vol. 32, No. 1, (2017), 348–358. doi:10.1109/TEC.2016.2624219
3. Ghaheri, A., Mohammadi Ajamloo, A., Torkaman, H., and Afjei, E., "Design, modelling and optimisation of a slot-less axial flux permanent magnet generator for direct-drive wind turbine application", ***IET Electric Power Applications***, Vol. 14, No. 8, (2020), 1327–1338. doi:10.1049/iet-epa.2019.0385
4. Bhuiyan, N. A., and McDonald, A., "Optimization of Offshore Direct Drive Wind Turbine Generators With Consideration of Permanent Magnet Grade and Temperature", ***IEEE Transactions on Energy Conversion***, Vol. 34, No. 2, (2019), 1105–1114. doi:10.1109/TEC.2018.2879442
5. Nasiri-Zarandi, R., Ghaheri, A., and Abbaszadeh, K., "Thermal Modeling and Analysis of a Novel Transverse Flux HAPM Generator for Small-Scale Wind Turbine Application", ***IEEE Transactions on Energy Conversion***, Vol. 35, No. 1, (2020), 445–453. doi:10.1109/TEC.2019.2936683
6. Moradi CheshmehBeigi, H., "Design, Optimization and FEM Analysis of a Surface-Mounted Permanent-magnet Brushless DC Motor", ***International Journal of Engineering***, Vol. 31, No. 2, (2018), 339–345. doi:10.5829/ije.2018.31.02b.19
7. Zahabi, M., Ardeshir, G., and Ale Ahmad, A., "Influence of DC-Link Voltage on Commutation Torque Ripple of Brushless DC Motors with Two-Segment Pulse-width Modulation Control Method", ***International Journal of Engineering - Transaction B: Applications***, Vol. 31, No. 2, (2018), 307–314. doi:10.5829/ije.2018.31.02b.15
8. Torkaman, H., Ghaheri, A., and Keyhani, A., "Design of Rotor Excited Axial Flux-Switching Permanent Magnet Machine", ***IEEE Transactions on Energy Conversion***, Vol. 33, No. 3, (2018), 1175–1183. doi:10.1109/TEC.2018.2807804
9. Husain, T., Hasan, I., Sozer, Y., Husain, I., and Muljadi, E., "Design Considerations of a Transverse Flux Machine for Direct-Drive Wind Turbine Applications", ***IEEE Transactions on Industry Applications***, Vol. 54, No. 4, (2018), 3604–3615. doi:10.1109/TIA.2018.2814979
10. Ajamloo, A. M., Ghaheri, A., and Nasiri-Zarandi, R., "Design and Optimization of a New TFPM Generator with Improved Torque Profile", 2019 International Power System Conference (PSC), IEEE, (2019), 106–112. doi:10.1109/PSC49016.2019.9081559
11. Ueda, Y., and Takahashi, H., "Transverse-Flux Motor Design With Skewed and Unequally Distributed Armature Cores for Reducing Cogging Torque", ***IEEE Transactions on Magnetics***, Vol. 53, No. 11, (2017), 1–5. doi:10.1109/TMAG.2017.2703087
12. Wang, Q., Zhao, B., Zhao, H., Li, Y., and Zou, J., "Optimal Design of Tubular Transverse Flux Motors With Low Cogging Forces for Direct Drive Applications", ***IEEE Transactions on Applied Superconductivity***, Vol. 26, No. 7, (2016), 1–5. doi:10.1109/TASC.2016.2600104
13. Washington, J. G., Atkinson, G. J., and Baker, N. J., "Reduction of Cogging Torque and EMF Harmonics in Modulated Pole Machines", ***IEEE Transactions on Energy Conversion***, Vol. 31, No. 2, (2016), 759–768. doi:10.1109/TEC.2016.2520200
14. Nasiri-Zarandi, R., Ajamloo, A. M., and Abbaszadeh, K., "Design Optimization of a Transverse Flux Halbach-Array PM Generator for Direct Drive Wind Turbines", ***IEEE Transactions on Energy Conversion***, Vol. 35, No. 3, (2020), 1485–1493. doi:10.1109/TEC.2020.2975259
15. Nasiri-Zarandi, R., Ghaheri, A., and Abbaszadeh, K., "Cogging Torque Reduction in U-Core TFPM Generator Using Different Halbach-Array Structures", 2018 International Symposium on Power Electronics, Electrical Drives, Automation and Motion (SPEEDAM), IEEE, (2018), 1153–1158. doi:10.1109/SPEEDAM.2018.8445328
16. Liu, C., Zhu, J., Wang, Y., Lei, G., and Guo, Y., "Cogging Torque Minimization of SMC PM Transverse Flux Machines Using Shifted and Unequal-Width Stator Teeth", ***IEEE Transactions on Applied Superconductivity***, Vol. 26, No. 4, (2016), 1–4. doi:10.1109/TASC.2016.2543959
17. Dobzhanskyi, O., Gouws, R., and Amiri, E., "Analysis of PM Transverse-Flux Outer Rotor Machines With Different Configuration", ***IEEE Transactions on Industry Applications***, Vol. 53, No. 5, (2017), 4260–4268.

doi:10.1109/TIA.2017.2696901

18. Gieras, J. F., "Performance Characteristics of a Transverse Flux Generator", IEEE International Conference on Electric Machines and Drives, 2005, IEEE, (2005), 1293–1299. doi:10.1109/IEMDC.2005.195889
19. Azari, M. N., "Performance Improvement of a Slotted Solid Rotor Induction Motor with High Temperature Superconder Coating", ***International Journal of Engineering - Transaction B: Applications***, Vol. 32, No. 5, (2019), 693–700. doi:10.5829/ije.2019.32.05b.11
20. Fekri, H., Shamsi-Nejad, M., and Hasheminejad, S., "Performance Analysis of a Novel Three-phase Axial Flux Switching Permanent Magnet Generator with Overlapping Concentrated Winding", ***International Journal of Engineering - Transaction B: Applications***, Vol. 32, No. 2, (2019), 286–295. doi:10.5829/ije.2019.32.02b.14
21. Ostovic, V., "Dynamics of saturated electric machines", Springer Science & Business Media, (2012).
22. Nasiri-Zarandi, R., Ajamloo, A. M., and Abbaszadeh, K., "Proposing the Output Equations and 3-D MEC Modeling for U - Core TFPM Generators", 2018 International Symposium on Power Electronics, Electrical Drives, Automation and Motion (SPEEDAM), IEEE, (2018), 292–297. doi:10.1109/SPEEDAM.2018.8445324
23. Sudhoff, S.D., "Power magnetic devices: A multi-objective design approach", John Wiley & Sons, (2014).
24. Mohammadi Ajamloo, A., Ghaheri, A., Shirzad, H., and Afjei, E., "Non-linear analytical modelling and optimisation of a 12/8 rotor excited flux-switching machine", ***IET Electric Power Applications***, Vol. 14, No. 9, (2020), 1592–1603. doi:10.1049/iet-epa.2019.0732
25. Ghorbani, S., and Reaz Kashyzadeh, K., "Taguchi Approach and Response Surface Analysis for Design of a High-performance Single-walled Carbon Nanotube Bundle Interconnects in a Full Adder", ***International Journal of Engineering - Transaction B: Applications***, Vol. 33, No. 8, (2020), 1598–1607. doi:10.5829/ije.2020.33.08b.18
26. Mohammadi Ajamloo, A., Abbaszadeh, K., and Nasiri-Zarandi, R., "A Novel Transverse Flux Permanent Magnet Generator for Small-Scale Direct Drive Wind Turbine Application: Design and Analysis", ***Scientia Iranica***, (2019). doi:10.24200/sci.2019.53145.3078

Persian Abstract

چکیده

ماشین‌های آهنربای دایم شارمتقاطع گونه‌ای از ماشین های سنکرون هستند که از چگالی گشتاور زیادی برخوردارند و قابلیت جای دادن تعداد قطب های زیادی را دارا هستند. این دو خصوصیت منجر می‌شود تا ماشین‌های شارمتقاطع گزینه مناسبی برای کاربردهای کم سرعت با چگالی گشتاور بالا از جمله توربین بادی وصل مستقیم باشند. علیرغم مزایای نام برده، ماشین‌های شارمتقاطع به طور ذاتی از گشتاور دندانه زیاد رنج می‌برند که ویژگی نگران‌کننده‌ای در توربین‌های بادی وصل مستقیم می‌باشد. هدف این مقاله، کمینه کردن گشتاور دندانه این ماشین‌ها با استفاده از روش تکه کردن آهنربا در جهت محوری می‌باشد. مفهوم این روش پیشنهادی با استفاده از روش‌های تحلیلی بیان شده و میزان اختلاف زاویه بهینه آهنرباها در یک فرمول جامع استخراج شده است. روش مدار معادل مغناطیسی غیرخطی در این مقاله به کار گرفته شده است که در آن اثر تکه کردن آهنربا، عکس العمل آرمیچر، گردش روتور و اشباع هسته آهن به دقت مدل شده است. همچنین، نتایج تحلیل مدار معادل مغناطیسی با نتایج روش المان محدود از حیث دقت و زمان شبیه‌سازی مقایسه شده است. نتیجه مقایسه حاکی از آن است که روش مدار معادل مغناطیسی پیشنهادی زمان شبیه‌سازی را تا 10 برابر نسبت به روش المان محدود کاهش داده و از میزان دقت قابل قبولی برخوردار می‌باشد. سپس روش بهینه‌سازی تاگوچی به عنوان یکی از روش‌های بهینه‌سازی پرسرعت بکار گرفته شده است تا مشخصات گشتاور ژنراتور شار متقاطع را بهبود ببخشد. نتایج بهینه‌سازی حاکی از آن است که با استفاده از روش پیشنهادی این مطالعه و انجام فرآیند بهینه‌سازی، گشتاور دندانه ژنراتور 97 درصد کاهش پیدا کرده است درحالی که گشتاور میانگین حدود 8 درصد افت نموده است که با توجه به افت قابل توجه گشتاور دندانه، می‌تواند به عنوان یک اثر جانبی، قابل تحمل باشد.